Journal of the Optical Society of Korea, Vol 5, No. 1, March 2001, pp. 9-15

Study on the First On-Orbit Solar Calibration Measurement of Ocean Scanning Multi-spectral Imager (OSMI)

Young-Min Cho*

Korea Aerospace Research Institute, Taejon 305-600, KOREA

(Received June 7, 2000)

The ocean Scanning Multi-spectral Imager (OSMI) is a payload on the KOrea Multi-Purpose SATellite (KOMPSAT) to perform worldwide ocean color monitoring for the study of biological oceanography. OSMI performs solar and dark calibrations for on-orbit instrument calibration. The purpose of the solar calibration is to monitor the degradation of imaging performance for each pixel of 6 spectral bands and to correct the degradation effect on OSMI image during the ground station data processing. The design, the operation concept, and the radiometric characteristics of the solar calibration are investigated. A linear model of image response and a solar calibration radiance model are proposed to study the instrument characteristics using the solar calibration data. The first on-orbit solar calibration data are analyzed for the initial check up of the on-orbit instrument performance of spectral responsivity and spatial response uniformity. The first solar calibration data and the analysis results are important references for further study on the on-orbit stability of OSMI response during its lifetime.

OCIS codes : 010.0010, 110.0110, 120.0120.

I. INTRODUCTION

The study of worldwide phytoplankton distribution in the ocean can give knowledge of primary ocean production (i.e. algae and some bacteria) and of global biochemistry such as the ocean's role in the global carbon cycle. The concentration of phytoplankton can be derived from satellite observation of ocean color. This is because ocean color in the visible light region (wavelengths from 400 nm to 700 nm) varies with the concentration of chlorophyll and other plant pigments in the water. For example, chlorophytes and diatoms absorb light at wavelengths below 550 nm, phycocerythin absorption peaks around 490 nm, and gelbstoffe absorbs below 550 nm.

After the ocean data from the Coastal Zone Color Scanner (CZCS) on Nimbus-7 were found to be useful for global study of the ocean [1,2], several advanced ocean monitoring sensors were launched, are operating currently, or are to be launched in the near future such as OCTS (Japan), MOS (German), SeaWiFS (USA), OCI (Taiwan), MODIS (USA), MERIS (ESA), GLI (Japan).

The Ocean Scanning Multi-spectral Imager (OSMI) [3,4] is the first Korean ocean monitoring space-borne instrument, developed by the Korea Aerospace Research Institute (KARI) and TRW, Inc (USA). OSMI is accommodated on the KOrea Multi-Purpose SATellite (KOMPSAT) which was launched successfully to a 685 km sun synchronous orbit on 21 December, 1999 (Korean standard time) [5,6]. OSMI is operated by KARI. Since the main aperture cover of OSMI was opened on January 16, 2000, OSMI has gathered on-orbit calibration and ocean image data for the initial check up of on-orbit instrument functionality and performance, as planned.

OSMI performs solar and dark calibrations for on-orbit instrument calibration. The combination of the dark calibration and the solar calibration measurements can be used to monitor the on-orbit stability of the OSMI response (the relative response to the initial on-orbit value) over the 3 year mission life. The first on-orbit calibration data are important references for the study of the OSMI response stability. The operational concept and the radiometric characteristics of the solar calibration are investigated. The first on-orbit solar calibration measurement data are analyzed in terms of relative values and compared with theoretical predictions and pre-launch laboratory measurements [7] for the sake of the initial check up of the on-orbit instrument performance such as the spectral responsivity and spatial response uniformity.

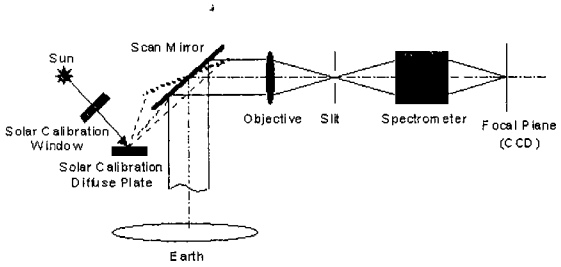

FIG. 1. The schematic diagram of OSMI optics for imaging and solar calibration.

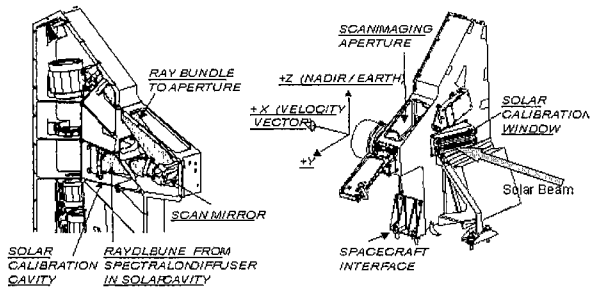

FIG. 2. The structure of OSMI solar calibration window and cavity.

II. SPECTRAL BAND AND MISSION OPERATION

The mission goal of OSMI is to perform world-wide ocean color monitoring for the study of biological oceanography. For the sake of flexible mission OSMI has on-orbit spectral band selectability and programmable gain and offset. After launch any 6 spectral bands can be selected at a time in the spectral range from 400 nm to 900 nm via ground station command. Since it is practically impossible to measure performance for all of the thousands of possible bands, the instrument performance was measured for the 8 primary spectral bands (See Table 1.) during its development. The OSMI ocean color spectral bands B0 through B4 provide ocean color data while band B5, BX and B6 provide information for atmospheric (aerosol) corrections. During routine on-orbit operation, the 6 bands B0, B1, B2, B4, BX, and B6 are selected among the 8 bands for compatibility with the OSMI image data processing software of the KARI ground station [8].

OSMI performs a whisk-broom scan for imaging operation with the ground sample distance of 1 km and the ground swath width of 800 km during a 20 % duty cycle. The optical images of 6 spectral bands collected by OSMI optics are converted to analog electric signals by a Charge Coupled Device (CCD) on the focal plane assembly. The analog signal is digitized to a 10-bit gray level after analog gain and offset adjustment and then is losslessly compressed before transfer to the payload data transmission subsystem for down load to the KARI ground station or on-orbit storage.

OSMI has a 2-dimensional CCD that has 96 pixels along the spatial direction and 192 pixels along the spectral direction. The CCD pixels are divided into two groups along the spatial direction. One is called '(−) field' which includes 48 spatial pixels forward of the satellite velocity direction, the other is '(+) field' which includes 48 backward spatial pixels. Each field has a different CCD quantum efficiency so that the radiometric response characteristics at two fields are different for all the bands.

III. OSMI SOLAR CALIBRATION DESIGN AND OPERATION

The purpose of the solar calibration is to monitor the on-orbit degradation of imaging performance such as instrument aging effect and to correct the degradation effect on the OSMI ocean image for each pixel of all the spectral bands. For the realization of this purpose OSMI is designed to have two key components, the solar calibration window and the calibration diffuse plate as shown in Figs. 1 and 2. The window is made of 5 thick slits. The slits attenuate the intensity of the solar beam going through them to provide solar

TABLE 1. OSMI primary spectral bands.

Spectral Band	Band Center (nm)	Bandwidth (nm)	Sensing Objective
B0	412	20	Desolved Organic Material, Aerosol
B1	443	20	Concentration of chlorophyll
B2	490	20	Concentration of pigment
B3	510	20	Turbidity of chlorophyll
B4	555	20	Turbidity
B5	670	20	Calibration of atmospheric effect
BX	765	40	Calibration of atmospheric effect
B6	865	40	Calibration of atmospheric effect

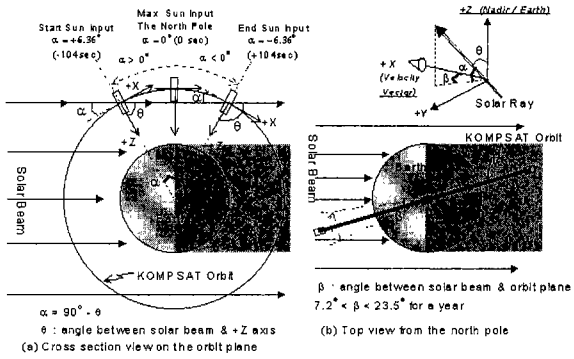

FIG. 3. OSMI solar calibration operation concept.

input radiance values that approximate ocean scene input radiance. The diffuse plate is a white diffuse reflector made of a space grade Spectralon by Labsphere Inc.. The plate is mounted in a metal holder inside the solar calibration cavity, so that the scan mirror views the target diffusing the attenuated solar beam uniformly to all directions.

The solar calibration data are acquired once every orbit near the Earth North Pole. Two dark calibrations are activated before and after the solar calibration for the dark signal correction of the solar calibration signal. The solar calibration output signal depends on the direction of the solar ray bundle incident to the calibration window. The direction is expressed in terms of the angles of α and β defined in the Fig. 3. Assuming perfect satellite attitude control, the angle α is for the variation of the solar ray incidence direction due to the satellite orbital movement during one orbit and the angle β is due to the seasonal variation of the orbit plane.

IV. THEORETICAL ANALYSIS OF OSMI SOLAR CALIBRATION RESPONSE

Since the photon detector CCD has almost linear response to input light amount, the solar calibration output signal after dark signal correction S_c can be modeled as the following linear equation.

$$S_c = S_s - S_d = g_1 \times R_s + g_0, \qquad (1)$$

where S_s is solar calibration output signal, S_d is dark calibration output signal, R_s is solar input radiance ($\mathrm{Wm^{-2}Sr^{-1}\mu m^{-1}}$), g_1 and g_0 are linear radiometric response coefficients of OSMI imaging system that are interpreted as response gain [counts/($\mathrm{Wm^{-2}Sr^{-1}\mu m^{-1}}$)] and response shift [counts] respectively.

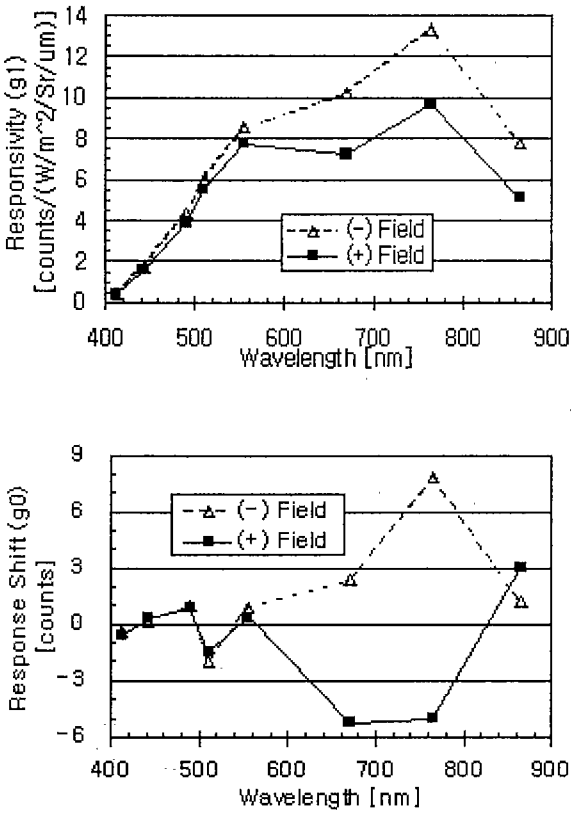

FIG. 4. The coefficients of OSMI radiometric response at the minimum gain setting.

It was reported by TRW [7] that the coefficients g_1 and g_0 are obtained for each spectral band and each field by linear curve fitting to the laboratory performance measurement data taken at the minimum gain setting under the ambient environment before launch (Fig. 4). In the pre-launch measurement a broad band lamp and monochromator was used for the light source. The radiance of the input beam was measured by using the pyroelectric reference detector that was calibrated with traceablility to the radiometric standard of the National Institute of Standards and Technology in the USA. The scan mirror of OSMI was fixed to look at the nadir direction (+Z axis in the Fig. 2). Output signal of OSMI was recorded as the input radiance was increased in several steps below the OSMI saturation level. The radiometric response coefficients were calculated using the input radiance values and the corresponding output signal after the subtraction of the dark calibration output signal.

The solar input radiance (R_s) can be expressed in terms of the function of wavelength λ, solar angle α and β, and time t as

$$R_s(\lambda, \alpha, \beta, t) = I_s(\lambda, t) T_{sw}(\alpha) \times BRDF(t) \cos\alpha \cos(65^\circ - \beta), \qquad (2)$$

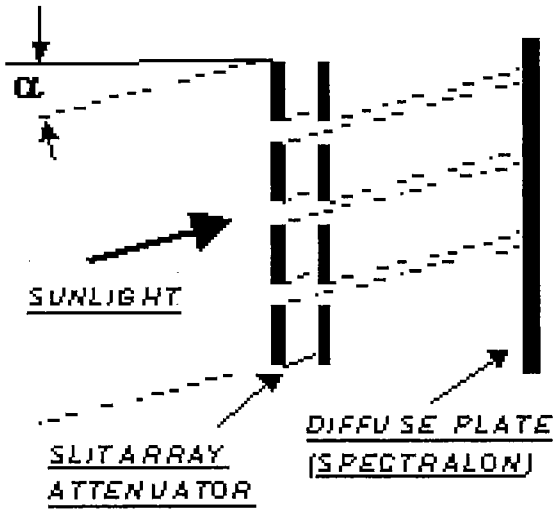

FIG. 5. Light attenuation of solar window

where $I_s(\lambda, t)$ is solar irradiance incident into the solar calibration window, $T_{sw}(\alpha)$ is light transmittance of the solar calibration window, $BRDF(t)$ is the Bidirectional Reflectance Distribution Function of the Spectralon.

The solar irradiance $I_s(\lambda, t)$ depends mainly on wavelength and the Earth-Sun distance [9] as

$$I_s(\lambda, t) = I_m(\lambda) \times [1 + 0.0167 \cos(2\pi(D-3)/365)]^2, \quad (3)$$

where $I_m(\lambda)$ are the mean extraterrestrial irradiance values [10], $D = D(t)$ is the sequential day of the year.

The mean irradiance values are corrected to the effective mean solar irradiance values which are spectrally weighted over all of the OSMI bandwidths using the laboratory measured intra-band spectral responsivity (Table 2).

The window light transmittance $T_{sw}(\alpha)$ can be formulated into the Eq. (4) from understanding the design of the solar calibration window and cavity structure.

$$T_{sw}(\alpha) = (0.042 - 0.383 \tan\alpha)/0.192. \quad (4)$$

When the solar beam makes normal incidence to the window surface, the window gives the maximum light transmittance of 22 %. Fig. 5 illustrates that the transmittance decreases as the absolute value of the angle α increases.

It is reported by the manufacturer of the Spectralon, Labsphere, Inc. that the Spectralon reflectance has been shown to degrade less than 4 % at 400 nm and less than 1 % at 900 nm after 100 hours of equivalent UV/VUV radiation found in low earth orbit. So, OSMI is designed to limit the total accumulated equivalent normal sun falling on the Spectralon to 87 hrs for the 3 year mission life. This can mean the OSMI Spectralon reflectance can be degraded about 0.1 % at 400 nm and about 0.02 % at 900 nm every month. Based on the measurement data of the spectral 8deg. hemispherical reflectance factor with the random uncertainty less than 0.5 % by Labsphere, Inc., the spectral variation of the BRDF is within 0.5 % at the range of 400 $\sim$ 900 nm.

During one orbit solar calibration time, the temporal variation of the solar irradiance, the Spectralon reflectance and the orbit plane direction can be ignored, and we can assume the angle β and $BRDF$ are constant. For enough high input radiance, g_0 can also be ignored so that the solar calibration signal can be approximated by

$$S_c(\lambda, x, t) \sim g_1(\lambda, x) I_m(\lambda) T_{sw}(\omega t) \cos(\omega t) \times BRDF \cos(65^\circ - \beta), \quad (5)$$

where ω is the orbital angular velocity of the satellite and the solar angle $\alpha = \omega t$.

For a spectral band and a spatial pixel, during one orbit, the temporal variation of the solar calibration signal normalized to the value at the time $t = 0$ follows mainly the light transmittance of the solar window as the Eq. (6).

$$S_c(t)/S_c(0) \sim T_{sw}(\omega t)/T_{sw}(0) \times cos(\omega t). \quad (6)$$

For a time and a spatial pixel, the spectral variation of the solar calibration signal normalized to the value at the band wavelength of λ_0 depends on the normal-

TABLE 2. The mean extraterrestrial solar irradiance.

Spectral Band	B0	B1	B2	B3	B4	B5	BX	B6
Wavelength (nm)	412	443	490	510	555	670	765	865
Mean Solar Irradiance $I_m(\lambda)$ [$Wm^{-2}\mu m^{-1}$]	1713.9	1890.5	1947.3	1874.5	1860.8	1536.1	1227.0	980.9
(−) Field Effective Mean Solar Irradiance $I_m(\lambda)$	1702.6	1866.8	1949.0	1879.3	1861.4	1536.7	1227.1	980.6
(+) Field Effective Mean Solar Irradiance $I_m(\lambda)$	1702.6	1866.8	1949.0	1878.2	1861.3	1536.6	1227.0	980.6

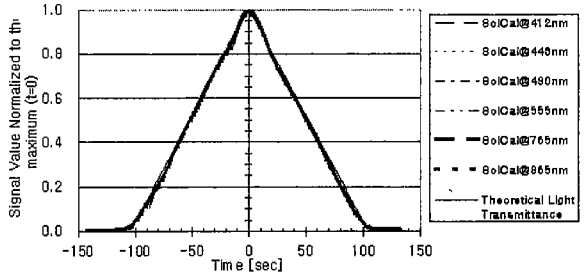

FIG. 6. Temporal variation of solar calibration signal at the 25th pixel.

ized product of the solar irradiance spectrum function and the spectral responsivity of OSMI imaging system as the Eq. (7).

$$S_c(\lambda)/S_c(\lambda_0) \sim \frac{g_1(\lambda) \times I_m(\lambda)}{g_1(\lambda_0) \times I_m(\lambda_0)}. \quad (7)$$

For a time and a spectral band, the spatial variation of solar calibration signal normalized to the value at the pixel position x_0 depends on the spatial response uniformity of OSMI imaging system as the Eq. (8).

$$S_c(x)/S_c(x_0) \sim g_1(x)/g_1(x_0). \quad (8)$$

V. THE FIRST ON-ORBIT OSMI SOLAR CALIBRATION MEASUREMENT

The first on-orbit solar calibration measurement data were taken at the bands of B0, B1, B2, B4, BX, B6 and the minimum gain setting during 5 minutes 3 January 2000 around the Earth north pole. After the dark signal correction using the dark calibration data acquired before and after the solar calibration, the three major characteristics of the solar calibration signal are investigated as the following.

The 25^{th} pixel shows for all 6 bands in Fig. 6 that the temporal variation of the solar calibration data during one orbit is very close to the theoretical prediction of the solar calibration light transmittance of Eq. (4) as stated in Eq. (6). The deviation of the normalized temporal solar calibration signal from the theoretical prediction value is shown in terms of root mean square value for the 6 bands in Table 3. For the 25th pixel of (−) field and the 73rd pixel of (+) field, at $\alpha = 1.217$ deg ($t = -20$ sec), the spectral variation

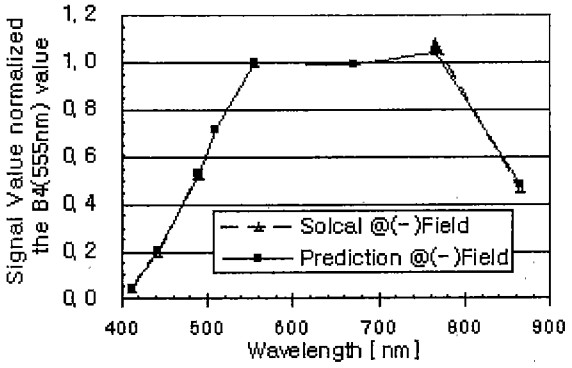

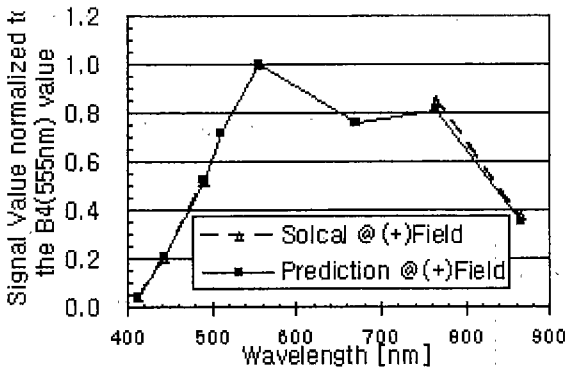

FIG. 7. Spectral behavior of solar cal. signal at the (−) field (25th pixel) and the (+) field (73rd pixel).

of the on-orbit solar calibration among the 6 bands is also very close to the theoretical prediction based on the solar irradiance of Table 2 and the prelaunch instrument responsivity of Fig. 4 as mentioned in Eq. (7) (Fig. 7). For each of the 6 bands, the spatial variation of the on-orbit solar calibration at $\alpha = 1.217$ deg ($t = -20$ sec) is analyzed and compared with the prelaunch spatial response uniformity of OSMI imaging system measured by TRW laboratory per Eq. (8) (Fig. 8). Noted are the big differences between the solar calibration data and the laboratory data at the (+) field pixels for the bands of B0, B1, and B2 and around the 40^{th} pixel for all the bands. As some possible reason, it can be considered that the differences come from the environment difference between two measurements, lack of laboratory measurement data in the short wavelength bands, and change in pixel

TABLE 3. The deviation of the normalized temporal solar calibration signal from the theoretical value.

Wavelength	412 nm	443 nm	490 nm	555 nm	765 nm	865 nm
Root mean square of the deviation	0.026	0.021	0.020	0.019	0.018	0.019

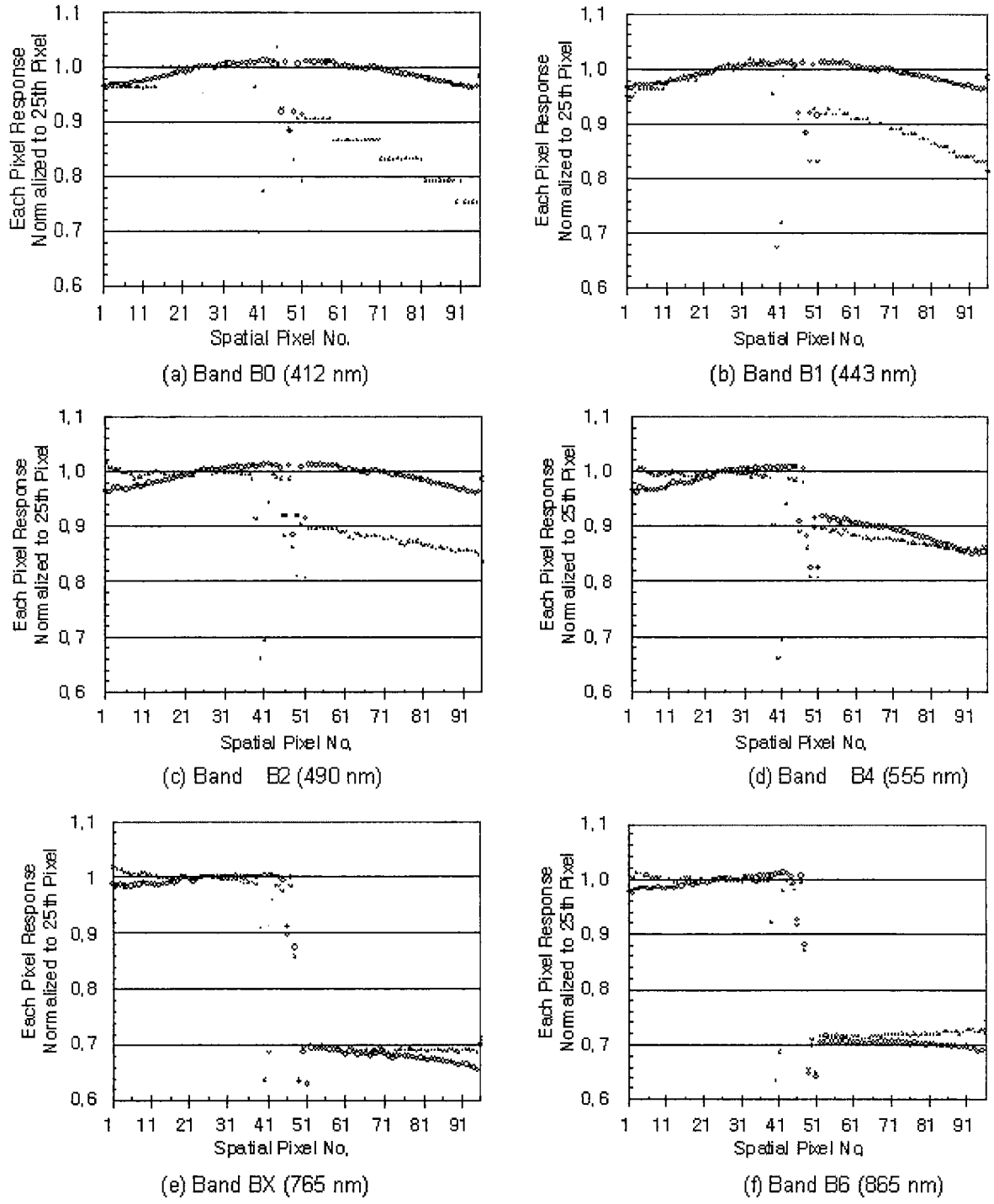

FIG. 8. Spatial variation of solar calibration and laboratory spatial pixel response uniformity. (O : Laboratory measurement before launch, X : Solar calibration after launch).

characteristics since the laboratory measurement [4,7]. All the changes from pre-launch to post-launch are reflected in the first on-orbit calibration measurement. This is why the on-orbit calibration is required and used for the image correction.

VI. CONCLUSION

The design, the operational concept and the radiometric characteristics of the solar calibration are investigated. The linear model of image response and the solar calibration radiance model are proposed to study the instrument characteristics using the solar calibration data. The first on-orbit solar calibration measurement data are analyzed in terms of relative values for the initial check up of the instrument performance. The temporal variation and the spectral responsivity of the solar calibration data match well with theoretical predictions. The spatial response uniformity of the solar calibration is compared with the pre-launch laboratory measurement results. Most pixels show good match between the solar calibration and the pre-launch laboratory measurement. It is, however, noted that the spatial response uniformity in some pixels of some blue bands has changed since the pre-launch laboratory measurement.

This study tells how OSMI works after launch and what has changed from the pre-launch measurement. This is why the first solar calibration data are studied and should be used as the reference for further study on the on-orbit stability of OSMI response during its lifetime. This analysis also shows that the combination of the linear image response model and the solar calibration radiance model is a good starting point for the check up of the instrument performance and monitoring the degradation of OSMI on-orbit performance such as instrument aging effects. This study will be useful for the OSMI mission and operation planning, the OSMI image data calibration, and users' understanding about OSMI image quality.

ACKNOWLEDGMENTS

This work is a result of the KOMPSAT project funded by the Korean Ministry of Science and Technology and performed by Korea Aerospace Research Institute (KARI) and TRW. I appreciate the KARI payload team and ground station team as well as TRW engineers for their efforts on the KOMPSAT program.

*Corresponding author : ymcho@kari.re.kr.

REFERENCES

[1] C. R. McCLAIN, ECSC, EEC, EAEC, Brussels and Luxembourg (1993), 167.
[2] C. L. Leonard and C. R. McCLAIN, Int. J. Remote Sensing, **17**, 721 (1996).
[3] Y. M. Cho, S. S. Yong, S. G. Lee, S. H. Woo, K. H. Oh, and H. Y. Paik, in The Fifth International Conference on Remote Sensing for Marine and Coastal Environments, (San Diego, California, USA, 1998), I-459.
[4] Y. M. Cho,in International Symposium on Remote Sensing, (Kangnung, Korea, 1999), 390.
[5] S. R. Lee and H. J. Kim, in The third Asia-Pacific Conference On Multilateral Cooperation in Space Technology And Application, (Seoul, Korea, 1996), 199.
[6] M. J. Baek and Y. K. Chang, in The third Asia-Pacific Conference On Multilateral Cooperation in Space Technology And Application, (Seoul, Korea, 1996), 275.
[7] M. Frink, "KOMPSAT LRC FM Instrument End Item Data Package," TRW, February 13 (1998).
[8] Y. S. Kim, Y. S. Kim, H. S. Lim, D. H. Lee, and C. H. Kang, J. Korean Soc. of Remote Sensing, **15**, 357 (1999).
[9] H. R. Gordon, D. K. Clark, J. W. Brown, O. B. Brown, R. H. Evans, and W. W. Broenkow, Appl. Opt. **22**, 20 (1983).
[10] H. Neckel and D. Labs, J. Solar Physics, **90**, 205 (1984).